Available online at www.sciencedirect.com
ScienceDirect
Journal of the European Ceramic Society 31 (2011) 597–604
www.elsevier.com/locate/jeurceramsoc

Mesoscopic Monte Carlo simulations of interfacial films in ZnO–Bi_2O_3 ceramics

Benoit Coasne [a,*], Renaud Metz [a,b]

[a] *Institut Charles Gerhardt Montpellier, UMR 5253 CNRS, Université Montpellier 2, ENSCM, 8, rue de l'Ecole Normale, 34296 Montpellier Cedex 05, France*
[b] *Laboratoire Matériaux Energétiques et Composés Polyazotés, Lyon1-CNRS-Isochem (groupe SNPE), UMR 5179 CNRS/UCBL/CNES/SNPE, Université Claude Bernard–Lyon 1, Batiment Berthollet, 69622 Villeurbanne Cedex, France*

Received 30 April 2010; received in revised form 16 October 2010; accepted 30 October 2010
Available online 26 November 2010

Abstract

This paper reports mesoscopic Monte Carlo simulations (in which a 'mesoscopic particle' corresponds to a group of atoms or molecules) of interfacial films in ZnO–Bi_2O_3 binary ceramics. We observe the formation of Bi_2O_3-rich interfacial phases at the surface of ZnO grains (surface amorphous films) or at the grain-boundary between ZnO grains (intergranular films). In qualitative agreement with the experimental results reported on premelting of ceramics, the thickness of these films increases as the temperature increases up to the eutectic temperature. Moreover, the Bi_2O_3 concentration in the surficial or intergranular films is found to be larger than in the bulk. These surficial films exhibit both some layering and lateral ordering.

Keywords: Grain boundaries; Monte Carlo simulation; Surficial amorphous film (SAF); Intergranular film (IGF); Premelting

1. Introduction

Classical high voltage surge-protection devices, the so-called 'varistors', are binary ceramics which are synthesized by ball-milling more than 90 wt%. ZnO with other oxides such as Bi_2O_3, Sb_2O_3, Cr_2O_3, MnO and Co_3O_4.[1,2] After adding an organic binder, the aqueous slurry is spray-dried to produce particles which are then transferred to hydraulic pressing for shape forming. In a second step, the resulting green ceramics is sintered above 1100 °C to obtain a dense material having a heterogeneous microstructure which is at the origin of their non-ohmic electrical behavior (the 'varistor effect').[3,4] Upon sintering, a Bi_2O_3-rich phase, which arises from complex reactions between the multivalent dopants and additives, forms at the ZnO grain boundaries. The following chemical equilibrium reaction has been proposed to explain the formation of such an interfacial phase:

$$2Zn_2Bi_3Sb_3O_{14}(s) + 17ZnO(s) \leftrightarrows 3Zn_7Sb_2O_{12}(s) + 3Bi_2O_3(l) \quad (1)$$

where (s) and (l) denote solid and liquid phases, respectively. The nature of the intergranular rich phase varies along the grain boundary: from a several μm thick Bi_2O_3 amorphous film at the triple junction to a string of isolated bismuth ions at the homojunction[5] (Fig. 1). Such possible interfacial 'states', which arise from the abnormal grain growth of ZnO, are often referred to as 'complexions' in the literature.[6–8] As will be discussed later in this introduction, the stability of the different interfacial phases has been investigated by several groups. However, the relative stability of the Bi_2O_3 layer surrounding the ZnO grains with respect to the phase consisting of Bi-atoms into the ZnO matrix is not well understood because the binary phase diagram Bi_2O_3/ZnO itself remains unclear.[9,10] Moreover, in Bi_2O_3-doped ZnO, Bi_2O_3 might be present as complex phases such as "tetragonal β-Bi_2O_3" or "cubic γ-Bi_2O_3",[11] which cannot be easily distinguished by powder X-ray crystallography. Most of the discrepancies between the results reported in the literature

* Corresponding author. Tel.: +33 4 67 16 34 59.
E-mail addresses: benoit.coasne@enscm.fr, renaud.metz@univ-lyon1.fr (B. Coasne).

0955-2219/$ – see front matter © 2010 Elsevier Ltd. All rights reserved.
doi:10.1016/j.jeurceramsoc.2010.10.034

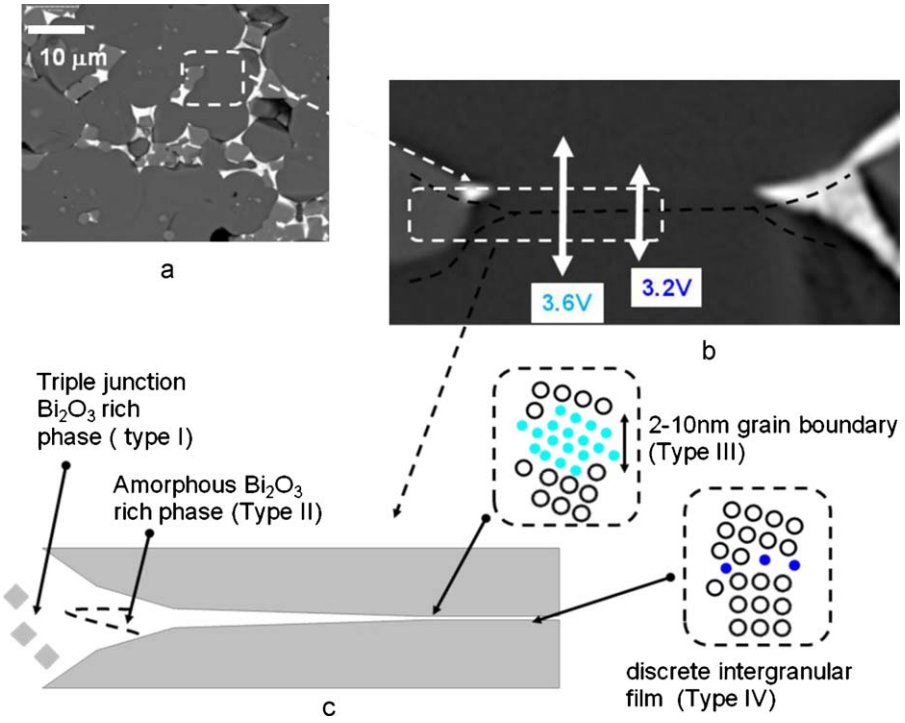

Fig. 1. (a) Backscatering electron image of a commercial ZnO varistor ceramic (the ceramic was courteously provided by Areva T&D). (b) ZnO/ZnO homojunction observed at high magnification with schematic illustrations of interfacial microstructures and their corresponding breakdown voltages as depicted in Ref. [19]. (c) Schematic representation of the interfacial microstructure after recession of Bi_2O_3 from the grain boundary to the triple points during the cooling of the ceramics.

can be partly explained by the differences in the experimental methods employed to investigate interfacial films in ceramics. On the one hand, X-ray diffraction, which is sensitive to phases having large volume fractions as it measures a large area of the sample, is unable to detect interfacial films. On the other hand, methods such as Transmission Electronic Microscopy (TEM) allow investigating junctions and interfacial films. Intergranular Bi-rich films at ZnO grain boundaries were observed by several authors such as Kingery et al.[12] or Greuter and Blatter[13] On the other hand, TEM images of the microstructure of commercial varistors show that most of the ZnO grains are not surrounded by a secondary-phase film.[5] The latter observation is in agreement with the work by Einzinger[14] who introduced the concept of homojunction (ZnO–ZnO junctions[2]). Metz et al.[5] also proposed that most of the Bi_2O_3 initial phase is in fact vaporized or solubilized in the ceramics. Other authors such as Gambino et al.[15] or Olsson and Dunlop[16] combined both views and proposed that the electrical properties of ZnO–Bi_2O_3 ceramics depend on their thermal history. In their work, Olsson and Dunlop[16] were able to show the existence of several interfaces in sintered polycrystalline ceramics: triple or multiple point interfaces with no varistor effect due to the presence of pyrochlore,[17] spinel interfaces with a moderate varistor effect (the latter finding is consistent with the fact that $Zn_7Sb_2O_{12}$ is a n-type semiconductor [18]), intergranular films of a thickness of 2 nm, and homojunctions with no intergranular phase but containing segregated Bi cations (corresponding to a partial coverage of ∼1/2 monolayer). We note that the formation of discrete partial monolayers has been confirmed by other groups and is considered as an equilibrium thickness in polycrystalline ZnO ceramics.[19,20] Among the interfacial phases mentioned above, the 2 nm thick Bi_2O_3 film was found to have the best electrical properties as far as the varistor effect is concerned[16]; indeed, such films have a 10% higher breakdown voltage compared to the Bi monolayer or 1/2 monolayer. A schematic illustration of a ceramics grain boundary based on the picture provided by the Olsson and Dunlop[16] and Kobayashi et al.[21] is presented in Fig. 1; two of the interfacial phases mentioned above can be observed: (1) Bi_2O_3-rich film having a thickness of several nm and (2) a 0.5 monolayer of atomic bismuth. From a theoretical point of view, *ab initio* calculations have shown that the decoration of ZnO grain boundaries by Bi atoms might occur as it is energetically favorable.[22] Other *ab initio* calculations by the same group[23] have also shown the low solubility of zinc in α-Bi_2O_3. However, the latter result is not supported by the experiments by Kumada et al.[24] who reported the synthesis at room temperature of the tetagonal-$ZnBi_2O_6$ and monoclinic-Bi_2O_4 phases. Regarding this last issue, it should be noted that *ab initio* calculations in Ref. [23] are 0 K calculations so that the entropy term, which significantly contributes to the solubility of foreign species, is neglected.

To gain insights into interfacial films in ZnO–Bi_2O_3 varistors, several studies have been carried out on ZnO sintering with Bi_2O_3 nanoparticles at temperatures close to the eutectic temperature of the binary system ($T_E \sim 740\,^\circ C$). These studies confirmed the formation of an interfacial amorphous film

having a constant thickness of 1.2 ± 0.3 nm.[19] Such surficial amorphous films (SAF), which correspond to a general phenomenon as they are also observed at the surface of oxides,[25,26] were explained by Luo and coworkers using a pressure-balance model.[27] In this thermodynamical approach, the stability of the SAF below the eutectic temperature is predicted by estimating the system free energy as the sum of volume and surface contributions. In the case of sintered ceramics, similar nanometric surficial films, the so-called intergranular films (IGF), are confined at the grain boundaries.[28] In the case of 'varistors', the IGF are thought to be at the origin of the varistor effect since Bi is required to observe the non-linear electric regime of the materials.[8] From a general point of view, the formation of SAF and IGF is described in the literature as a phenomenon in which premelting (the formation of these films is observed close to the eutectic temperature) combines with surface prewetting.[29–31] Despite the significant amount of work reported in the literature, some issues regarding the stability and formation of the Bi_2O_3-rich SAF and IGF still need to be addressed. Among the open questions, the nature of the driving force behind the formation of such films remain to be clarified: does it originate from the liquid surface tension between Bi_2O_3/ZnO(s) and/or from the confinement effect between ZnO grains? In order to gain insights into the formation of SAF and IGF in ZnO–Bi_2O_3 ceramics, we performed classical molecular simulations. Given the complexity of the system involved in the formation of the Bi-rich phase at the surface of a ZnO grain (SAF) or between two ZnO grains (IGF), we choose to conduct coarse-grained molecular simulations in which one considers mesoscopic particles consisting of a group of atoms or molecules (instead of considering explicitly each atom of the system as in fully atomistic simulations). Such mesoscopic simulations can be used to describe the thermodynamics and dynamics of large scale systems in a qualitative and efficient way. The main limitation of the mesoscopic methods lies in the fact that the details of the atomistic level are lost. As a result, it must be emphasized that the mesoscopic simulations employed in the present work do not account for all of the physical and chemical mechanisms behind the formation of SAF and IGF. In particular, the simple and ideal description of the interactions in our work does not account for the specific features (covalent bonding, ionic interaction, etc.) of any given experimental system. However, we believe that the present mesoscopic Monte Carlo simulations, with such a simple model, helps to shed light on the formation of interfaces in ceramics materials as it remains very general. In particular, the use of the semigrand ensemble, in which the fugacity of the ZnO and Bi_2O_3 phases as well as the pressure P and temperature T are fixed (more details will be provided in the computational section), allows estimating the Bi_2O_3-concentration and thickness of the SAF and IGF. By considering different temperatures T, we are thus able to draw a schematic phase diagram for the Bi-rich phase at the grain surface or boundary in varistor ceramics. In this paper, we report Monte Carlo molecular simulation in the semigrand canonical ensemble of (1) the formation of the Bi-rich interfacial phase at the surface of ZnO grains (SAF) and (2) at the grain boundary between ZnO grains (IGF).

2. Monte Carlo simulations in the semigrand canonical ensemble (NPTξ_B)

The Monte Carlo simulation technique in the semigrand canonical ensemble is a stochastic method based on Statistical Mechanics that simulates a binary system (AB) having a constant number of particles $N = N_A + N_B$ in equilibrium with an infinite reservoir of particles A and B imposing its fugacity fraction ξ_B (with $\xi_A + \xi_B = 1$) as well as its pressure P and temperature T.[32,33] The use of the semigrand canonical Monte Carlo simulation method was motivated by the fact that it is well adapted to estimate phase diagrams of binary systems.[34,35] The composition x_A is given by the ensemble average of the number N_A of particles A in the system over N. Monte Carlo trial moves in the semigrand canonical ensemble are particle displacements, volume changes, and particle exchanges, and obey the following acceptance probability:

$$P_{acc} = \min\left\{1, \exp\left[-\beta(U_N - U_O) - \beta P(V_N - V_O) + N \ln\frac{V_N}{V_O} + \lambda_{AB} \ln\frac{\xi_A}{1-\xi_B}\right]\right\} \quad (2)$$

where U_N and U_O, and V_N and V_O are the energies and volumes of the configuration after and before the move. $\beta = 1/k_B T$ where T is the temperature and k_B Boltzmann's constant. λ_{AB} equals 1 if the particle exchange attempt is from A to B and -1 if the particle exchange attempt is from B to A. Full details of the Monte Carlo technique in the semigrand ensemble can be found elsewhere.[32,34,35]

As stated above, the choice of the semigrand canonical ensemble was motivated by the fact that it allows estimating the composition of a mixture AB (ZnO and Bi_2O_3 in the present work) for a given fugacity fraction $\xi_{\equiv}$ (which is related to the activity coefficients of the phases), pressure P, and temperature T. In other words, Monte Carlo simulations in this ensemble can be employed to determine the composition of the system x_A as a function of pressure and temperature at a given fugacity fraction. We note that other common ensembles such as the canonical ensemble (in which N_A, N_B, V, and T are constant) and the isobar-isotherm ensemble (in which N_A, N_B, P, and T are constant) do not allow determining the change in the composition of the system when varying the temperature or pressure as N_A and N_B are maintained constant. On the other hand, we could have considered Monte Carlo simulations in the grand canonical ensemble (in which the chemical potentials μ_A and μ_B and V and T are constant) as N_A and N_B vary. We selected the semigrand ensemble as it allows considering molecular simulations for different temperatures T at a fixed pressure P (corresponding to the most common experimental situation in which the temperature and concentration are changed at a given pressure).

Due to the complexity of the system involved in the formation of the Bi-rich phase at the surface of a ZnO grain (SAF) or between two ZnO grains (IGF), fully atomistic simulation approaches are difficult to carry out. In contrast, mesoscopic simulations in which a 'particle' consists of a group of atoms or molecules allow describing the thermodynamics and dynamics

of large scale systems in a qualitative and efficient way (but, again, the details of the atomistic level are lost). In our work, both the ZnO (A) and Bi_2O_3 (B) phases are described as an assembly of 'particles' consisting of several atoms. The interaction energy between Bi_2O_3 (A) and ZnO (B) phases is modeled using Lennard–Jones potentials:

$$U_{ij}(r) = 4\varepsilon_{ij}\left\{\left(\frac{\sigma_{ij}}{r}\right)^{12} - \left(\frac{\sigma_{ij}}{r}\right)^{6}\right\} \quad (3)$$

where r is the distance between two particles i and j (i,j = A or B). The first term corresponds to the short range repulsive interaction when two particles overlap while the second term corresponds to the attractive van der Waals interaction that decays with the distance as r^{-6}. The interactions of Bi_2O_3/Bi_2O_3 and ZnO/ZnO were calculated using the following parameters in reduced units: $\sigma_{AA} = 1.0$, $\varepsilon_{AA} = 1.0$ and $\sigma_{BB} = 1.1765$, $\varepsilon_{BB} = 1.6$. The cross-species A/B parameters, $\sigma_{AB} = 1.0882$ and $\varepsilon_{AB} = 1.2649$, were calculated using the Lorentz–Berthelot combining rules. In what follows, all lengths and distances will be given in reduced units with respect to σ_{AA} while energies and temperatures will be given in reduced units with respect to ε_{AA}. These parameters were selected based on the fact that they lead to a simple eutectic binary solid (with a reduced eutectic temperature $T_E = 0.57$[34]) that is qualitatively similar to what is observed for ZnO/Bi_2O_3 ceramics. It is worth mentioning that the present model does not capture all of the features of grain boundaries and interfaces in ceramics as the details of the atomistic level are lost. Of particular importance, the specific interactions involved in ceramics such as the long-range ionic interaction and covalent bonding are not taken into account in our simulations. Due to such a limitation, we are aware that our model is not sophisticated enough to relate our results to a particular experimental example. Nevertheless, as will be shown later in this paper, this model can be applied to qualitatively predict the formation of SAF or IGF. We note that fully atomistic molecular simulations have been employed in the past to investigate impurity segregation in oxides[36] and IGF in ceramics.[37] Of particular interest for the present work, Yoshiya et al. investigated by means of energy minimization techniques (no temperature is considered in the calculations) the structure at the atomistic scale of an intergranular glassy film between two grains of silicon oxynitride.[37] In this pioneering work, the authors also considered the effect of the interface composition on its energy. In contrast to such seminal works on IGF, the present work does not allow determining the structure at the atomistic scale of SAF or IGF. On the other hand, the mesoscopic simulations considered in our work allows determining how the phase composition varies upon changing the pressure or temperature.

Three systems were considered in this work in order to investigate the formation of SAF and IGF in bulk binary solids (Fig. 2). A bulk sample consisting of a cubic box of $N = N_A + N_B = 4000$ particles was first considered. The initial configuration was constructed as a FCC crystal of a length $L \sim 18\sigma$. Particles were removed from the bulk sample in order to prepare a semi-infinite solid with a free interface (SAF initial configuration). In a similar fashion, particles were removed from the bulk sample in order to prepare two semi-infinite solids with free interfaces (IGF initial configuration). In the latter case, the spacing between the two semi-infinite solids is $2\sigma_{AA}$, Given the mesoscopic description considered in our model, we believe that we are not able to distinguish SAF and IGF at two grain junctions from those at triple of more junctions (being aware that the chemical features of the grain boundary phase depend on the type of junctions). As a result, in what follows, we restrict ourselves to the situations depicted in Fig. 2 in which a two-grain boundary or a free interface are considered. We also note that our model of IGF, which consists of two slabs separated by a short distance $2\sigma_{AA}$, does not capture the physical contact between grains in real samples. However, the present model can be used to mimic the confinement of atoms at the grain boundary. Moreover, in the course of the simulations, the atom positions are allowed to relax (see below) so that the final positions are separated by short distances which are comparable with those expected in grain boundaries.

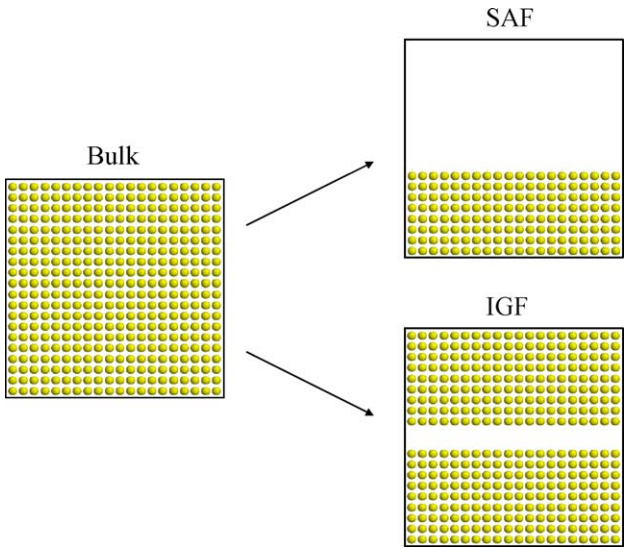

Fig. 2. Initial molecular configuration of a bulk binary system and of the SAF and IGF systems. The bulk sample is a cubic box of $N = 4000$ particles forming a FCC crystal of a length of $L \sim 18\sigma$. A free interface (SAF) is then prepared by removing particles from the bulk sample. In a similar fashion, particles were removed from the bulk sample in order to prepare two semi-infinite solids with free interfaces separated by a spacing of 2σ (IGF).

A cubic box was used to simulate the three systems shown in Fig. 2 since it is compatible with the FCC crystal stable phase of the Lennard–Jones mixtures AB.[37] Nevertheless, no numerical bias was used in the course of the simulations to impose this crystalline structure to remain stable; the initial FCC crystal structure was found to be stable as no melting was observed. Regular cubic boundary conditions were applied in the course of the simulation runs. Each simulation consisted of a first run to equilibrate the system using particle move and identity exchange attempts as well as volume change attempts. Once full equilibration is achieved, the system density ρ and composition x_A (which fluctuate around their equilibrium value) as well as density profiles $\rho(z)$ and pair correlation functions $g(r)$ were averaged in the course of a second simulation run. $\rho(z)$ is defined for each type of particles i (=A or B) from the average number of parti-

cles $<N_i(z)>$ with z between z and $z+\mathrm{d}z$:

$$\rho_i(z) = \frac{\langle N_i(z)\rangle}{L^2\,\mathrm{d}z} \tag{4}$$

The pair correlation function $g(r)$, which allows to determine whether the layer exhibits long-range (solid-like) or short-range (liquid-like) positional order, was calculated as:

$$g(r) = \frac{\langle N^p(r)\rangle}{\rho\pi r^2\,\mathrm{d}r} \tag{5}$$

where $\langle N^p(r)\rangle$ is the average number of pairs of particles located at a distance between r and $r+\mathrm{d}r$ from each other. The normalization factor in Eq. (4) corresponds to the number of molecules of an ideal gas having the density ρ in a system that would be comprised in the volume between r and $r+\mathrm{d}r$. In order to investigate the structure of the particles located at the free interface in the SAF and IGF, we calculated separately the $g(r)$ function for the particles in the bulk region of the material and that for the particles at the interface.

3. Results and discussion

Grain boundary melting has been investigated using either phase field theory[38,39] or molecular modeling such as Monte Carlo[40,41] or Molecular Dynamics[42–45] simulations. In contrast, the thermodynamical stability and structural properties of SAF or IGF in binary ceramics has received less attention. Fig. 3 presents our simulation results for the SAF and IGF as a function of the temperature. The subeutectic temperature was varied from $T=0.40$ up to 0.56 (the eutectic temperature is $T=0.57$). For each temperature, the fugacity fraction for ZnO was kept constant at $\xi_B=0.2$. Such a fugacity fraction and temperature range were selected for the following reasons. For these temperatures and fugacity, the bulk solid phase-separates into two solid regions A and B[34] as is observed for experimental Bi_2O_3–ZnO samples. Moreover, although changing the fugacity fraction and temperature range would lead to other quantitative values, the same qualitative behavior would be observed. This is the major limitation of any mesoscopic approach: while it allows considering large systems for a reasonable computing time and capturing the basic physics of the mechanisms, it is not quantitatively accurate as the details of the atomistic level are lost.

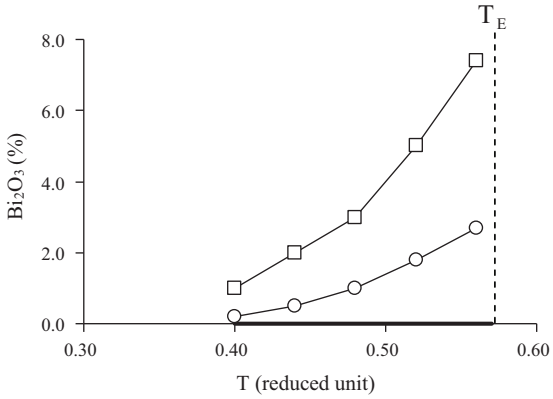

Fig. 3. Composition $x_{Bi_2O_3}$ of ZnO/Bi_2O_3 binary systems in various configurations as a function of temperature: (squares) SAF and (circles) IGF. The black thick line indicates the bulk composition $x_{Bi_2O_3}\sim 0$ while the dashed vertical line indicates the eutectic temperature, $T_E=0.57$.

Fig. 4 shows typical SAF and IGF configurations obtained at the subeutectic temperature $T=0.56$. In both cases, there is a film located at the free interfaces which is richer in Bi_2O_3 than the bulk region of the material. This result is in agreement with the work by Luo et al. who observed the formation of amorphous surficial films at the surface or at the grain boundaries in ceramic materials.[27] Fig. 3 shows the ZnO/Bi_2O_3 composition in the SAF and IGF configurations as a function of temperature. The composition was estimated by averaging the fraction of Bi_2O_3 particles over the whole thickness of the samples (consequently, the estimated value is necessarily lower than if the calculations were restricted to the outer layer of atoms in the SAF or IGF). For a given temperature, both $x_{Bi_2O_3}$ for the SAF and IGF are larger than that observed for the bulk ($x_{Bi_2O_3}\sim 0$). $x_{Bi_2O_3}$ varies from 1% up to 7% for the SAF as the temperature increases from $T=0.40$ up to 0.56. These results are consistent with the experimental data reported by Luo et al. who found that the Bi_2O_3 concentration is 18% in a SAF *versus* 0.023% in the bulk solid phase.[27] In contrast to the data for the SAF, $x_{Bi_2O_3}$ for the IGF varies from 0% up to 2% for the same temperature range. Interestingly, at a given temperature, the IGF composition lies in between those for the SAF and the bulk solid. This result suggests that the IGF is an intermediate situation between these two systems; atoms at the interface in the IGF can be seen as

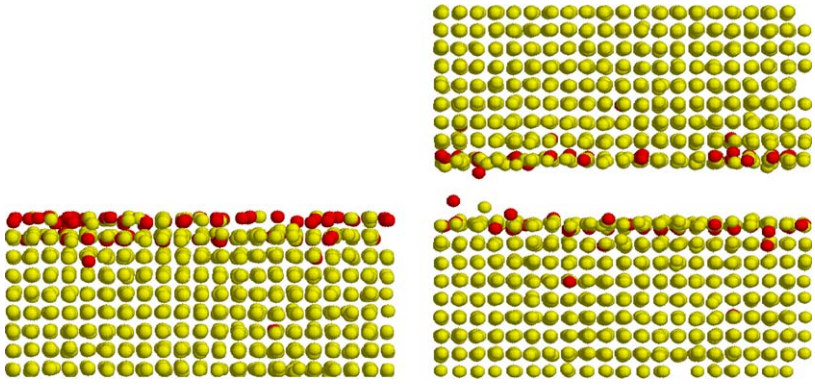

Fig. 4. Typical configuration for SAF (left) and IFG (right) at a temperature $T=0.56$ for a fugacity fraction $\xi_B=0.2$. Yellow and red spheres are the ZnO and Bi_2O_3 particles, respectively. (For interpretation of the references to color in this figure legend, the reader is referred to the web version of the article.)

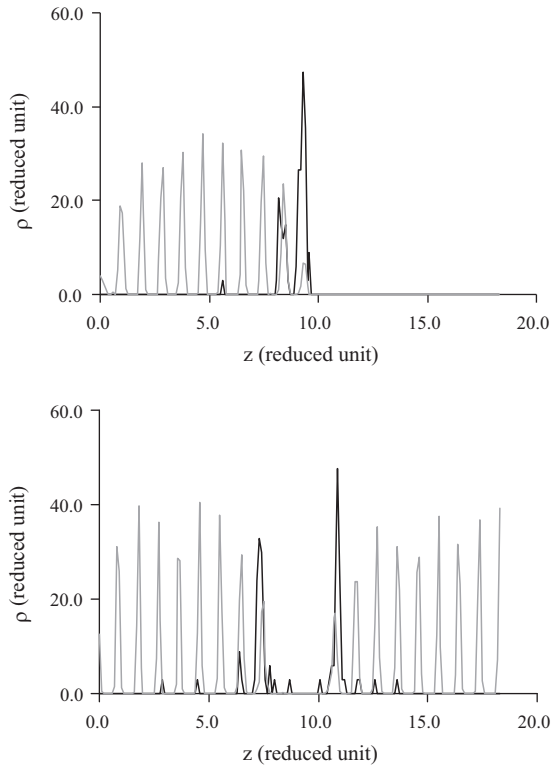

Fig. 5. Density profiles for ZnO/Bi_2O_3 binary systems at the subeutectic temperature $T = 0.56$ in various configurations: (top) SAF and (bottom) IGF. The black and grey lines are for Bi_2O_3 and ZnO, respectively. The density for ZnO has been divided by 10 for the sake of clarity.

forming a SAF but interacting with atoms or molecules belonging to the other semi-infinite solid. In order to get more insights into the formation and structure of SAF and IGF, we show in Fig. 5 the density profiles for these two systems at the subeutectic temperature $T = 0.56$. Both the contributions for Bi_2O_3 and ZnO are presented. Well-defined density peaks are observed due to the solid nature of the material at this subeutectic temperature.

In agreement with the molecular snapshots shown in Fig. 5, Bi_2O_3 particles are found to be located within about two layers at the interface. As in real experiments, defining the exact thickness of the SAF or IGF is a non-trivial task that necessarily lies on an arbitrary choice (about the location of the interface between the film and the bulk material for instance). As a first step, we have determined the thickness of the IGF or SAF film expressed as the number n_s of Bi_2O_3 molecules per unit of surface area (in reduced unit $\sigma_{AA}{}^2$). Table 1 reports the thickness n_s of the SAF and IGF as a function of the temperature T. For both films, n_s increases as the subeutectic temperature increases from $T = 0.40$ up to 0.56. Such a temperature-dependence of the film thickness is consistent with the experimental results reported for SAF.[19,20] Moreover, in agreement with our results above on the Bi_2O_3 concentration, it is found that the IGF thickness at a given temperature is about half that of the SAF. Again, this result is due to the fact that the IGF can be seen as intermediate between the SAF and the bulk material. In the case of the SAF, we further estimated the thickness of the film by fitting the amplitude of the

Table 1
Average thickness of the surficial film in ZnO/Bi_2O_3 binary systems as a function of temperature for the SAF and IGF. The eutectic temperature is $T_E = 0.57$. n_s is the surface density in reduced units (particles/$\sigma_{AA}{}^2$) while e is the thickness estimated from the simulation data using Eq. (9) (see text).

	SAF		IGF
	n_s	e	n_s
0.40	3.0	0.7	1.0
0.44	5.9	0.7	2.5
0.48	8.9	0.7	5.1
0.52	14.9	1.1	9.1
0.56	23.8	1.1	13.7

Bi_2O_3 density peaks using a decreasing exponential law:

$$A(j) = C \exp\left(-\frac{j}{e}\right) \quad (9)$$

where $A(j)$ is the amplitude of the jth density peak and C a constant. The characteristic length e, which corresponds to the penetration depth of Bi_2O_3 into the ZnO material can be used to estimate the SAF thickness. Table 1 shows e for the SAF as a function of temperature (e is expressed in reduced unit σ_{AA}). e varies from 0.7 at low temperature up to 1.1 at high temperature (close to the subeutectic temperature, $T_E = 0.57$). Assuming that σ_{AA} is of the order of magnitude of the nanometer (*i.e.*, a particle

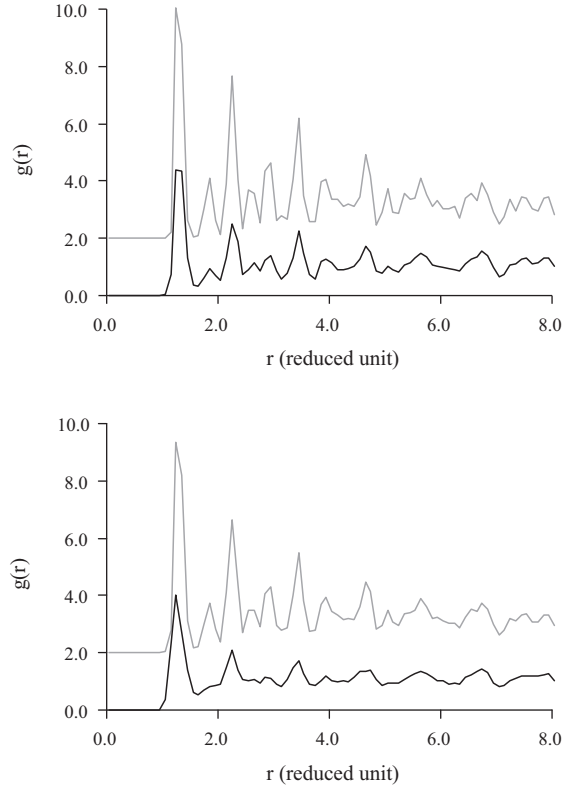

Fig. 6. Pair correlation functions $g(r)$ at two temperatures for ZnO/Bi_2O_3 binary systems in the SAF configuration: (top) $T = 0.40$ and (bottom) $T = 0.56$. The black and grey lines are for particles at the interface and those in the bulk region of the material, respectively. The pair correlation function for the bulk region has been shifted by +2 for the sake of clarity.

corresponds to a few Bi_2O_3 monomers), the values for e are consistent with those reported by Luo et al.[27] These authors found that below the eutectic temperature $T_E = 740\,^\circ C$ the film thickness increases from 0.96 nm at $T = 600\,^\circ C$ up to 1.30 nm at $T = 700\,^\circ C$.

In order to explore the structure of the SAF and IGF, the pair correlation function $g(r)$ was computed at low and high temperatures for the different configurations. Such pair correlation functions are useful to estimate the degree of positional ordering in the material. They provide similar information to that gained from the structure factor $S(q)$ measured in X-ray diffraction experiments [$g(r)$ and $S(q)$ are related through Fourier transformation]. Fig. 6 shows the $g(r)$ functions for particles in the bulk region of the material and for particles in the SAF (particles within the first two layers at the interface). The $g(r)$ functions for the IGF (results not shown for the sake of clarity) were found to be very similar to that for the SAF. As expected for temperatures below the eutectic temperature, significant positional ordering is observed for both the bulk and interfacial regions; (1) marked peaks appear at well defined positions and (2) long-range correlations are observed. The peaks become less marked as the temperature increases due to the fact that the thermal fluctuations increase. For each temperature, the SAF appears less ordered than the bulk material. This result can be explained by the fact that the less ordered particles in the SAF lead to a decrease in the interfacial energy of the configuration. Such a phenomenon is analogous to surface premelting, which corresponds to melting of atoms at the surface of a material at a temperature below the 3D melting temperature.[46] The observations above on the structure of SAF are consistent with the work by Luo et al.[25] who found that SAF exhibit some layering and lateral ordering.

4. Discussion and conclusion

In this paper, we investigated the formation of SAF and IGF in ZnO–Bi_2O_3 ceramics by means of mesoscopic molecular simulations (in which a 'particle' consists of a group of atoms or molecules). Although the simple and ideal description of the interactions considered in our work does not allow taking into account the specific features (covalent bonding, ionic interaction, etc.) of real binary ceramics, the present mesoscopic simulations provide a picture that qualitatively conforms to the experimental results. Moreover, the use of the semi-grand ensemble, in which the fugacity fraction of the ZnO and Bi_2O_3 phases as well as the pressure P and temperature T are fixed, allows estimating the Bi_2O_3-concentration and thickness of the SAF and IGF. By considering different temperatures T, we are thus able to draw a schematic phase diagram for the Bi-rich phase at the grain surface or boundary in ceramics.

Our results can be summarized as follows. The mesoscopic simulations show the formation of SAF and IGF below the bulk eutectic temperature. The thickness of these films is found to increase with increasing the temperature below the eutectic temperature, in qualitative agreement with the experimental results. Moreover, the Bi_2O_3 concentration in the films is much larger than in the bulk. It is also found that the IGF concentration falls in between that for the bulk and SAF, which suggests that the IGF is an intermediate situation between the SAF and the bulk material. Significant positional ordering is observed for the SAF or IGF. Such an ordering becomes less marked as the temperature increased due to increased thermal fluctuations. The results reported in the present paper are qualitatively consistent with previous experimental observations which have been interpreted on the basis of pressure balance thermodynamical approach.[27,30]

Acknowledgments

Calculations were performed using super-computers at the Institut de Développement et des Ressources en Informatique Scientifique (IDRIS, CNRS, grant No. 96223) and computers purchased thanks to funding from the French National Research Agency (ANR) through the research project "SIMONANOMEM" (ANR-07-NANO-055-04). We are grateful to the referee for his/her valuable comments, which helped us to improve the quality and clarity of our paper.

References

1. Clarke DR. Varistors ceramics. *J Am Ceram Soc* 1999;**82**:485–502.
2. Einzinger R. Metal-oxide varistors. *Ann Rev Mater Sci* 1987;**17**:299–332.
3. Bueno P, Varela J, Longo E. SnO_2, ZnO and related polycrystalline compound semiconductors: an overview and review on the voltage-dependent resistance (non-ohmic) feature. *J Eur Ceram Soc* 2008;**28**:505–29.
4. Glot AB. Non-ohmic conduction in oxide ceramics: tin oxide and zinc oxide varistors. In: Lin PB, editor. *Ceramic materials research trends*. Nova Science Publishers Inc; 2007. p. 227–73.
5. Metz R, Delalu H, Vignalou JR, Achard N, Elkhatib M. Electrical properties of varistors in relation to their true bismuth composition after sintering. *Mater Chem Phys* 2000;**63**:157–62.
6. Dillon SJ, Harmer MP. Multiple grain boundary transitions in ceramics: a case study of alumina. *Acta Mater* 2007;**55**:5247–54.
7. Dillon SJ, Tang M, Carter WC, Harmer MP. Complexion: a new concept for kinetic engineering in materials science. *Acta Mater* 2007;**55**:6208–18.
8. Dillon SJ, Harmer MP. Demystifying the role of sintering additives with complexion. *J Eur Ceram Soc* 2008;**28**:1485–93.
9. de la Rubia MA, Fernandez JF, Caballero AC. Equilibrium phases in the Bi_2O_3-rich region of the ZnO–Bi_2O_3 system. *J Eur Ceram Soc* 2005;**25**:2215–7.
10. Guha JP, Kunej S, Suvorov DJ. Phase equilibrium relations in the binary system Bi_2O_3–ZnO. *Mater Sci* 2004;**39**:911–8.
11. Onreabroy W, Sirikulrat N, Brown AP, Hammond C, Milne SJ. Properties and intergranular phase analysis of a ZnO–CoO–Bi_2O_3 varistor. *Solid State Ionics* 2006;**177**:411–20.
12. Kingery WD, Sande JB, Mitamura TJ. A scanning transmission electron microscopy investigation of grain-boundary segregation in a zinc oxide–bismuth oxide (Bi_2O_3) varistor. *J Am Ceram Soc* 1979;**62**:221–2.
13. Greuter F, Blatter G. Electrical properties of grain boundaries in polycrystalline compound semiconductors. *Semicond Sci Technol* 1990;**5**:111–37.
14. Einzinger R. Metal oxide varistor action—a homojunction breakdown mechanism. *Appl Surf Sci* 1978;**1**:329–40.
15. Gambino J, Kingery D, Pike G, Levinson L, Philipp HJ. Effect of heat treatments on the wetting behavior of bismuth-rich intergranular pahses in ZnO:Bi:Co varistors. *J Am Ceram Soc* 1989;**72**:642–5.
16. Olsson E, Dunlop GL. Characterization of individual interfacial barriers in a ZnO varistor material. *J Appl Phys* 1989;**66**:3666–75.
17. Clayton J, Takamura H, Metz R, Tuller HL, Wuensch BJ. The electrical and defect properties of $Bi_3Zn_2Sb_3O_{14}$ Pyrochlore: a grain-boundary phase in ZnO-based varistors. *J Electroceram* 2001;**7**:113–20.

18. Miyayama M, Kitagawa Y, Yanagida H. Electrical conduction in sintered Sb2/3Zn7/3O4 spinel. *J Mater Sci Lett* 1984;**3**:323–4.
19. Lee JR, Chiang YM. Bi segregation at ZnO grain boundaries in equilibrium with Bi_2O_3–ZnO liquid. *Solid State Ionics* 1995;**75**:79–88.
20. Luo J, Chiang YM. Equilibrium thickness amorphous film on {1 1 0} surfaces of Bi_2O_3-doped ZnO. *J Eur Ceram Soc* 1999;**19**: 691–7.
21. Kobayashi K, Wada O, Kobayashi M, Takad Y. Continuous existence of bismuth at grain boundaries of zinc oxide varistor without intergranular phase. *J Am Ceram Soc* 1998;**81**:2071–6.
22. Carlson JM, Hellsing B, Domingos HS, Bristowe PD. Theoretical investigation of the pure and Zn-doped α and δ phases of Bi_2O_3. *Phys Rev B* 2002;**65**:205122.
23. Carlson JM, Domingos HS, Hellsing B, Bristowe PD. Electronic structure of a Bi-doped $\Sigma = 13$ tilt grain boundary in ZnO. *Interface Sci* 2001;**9**:143–8.
24. Kumada N, Takahashi N, Kinomura N, Sleight AW. Preparation of ABi_2O_6 (A = MgZn) with the trirutile-type structure. *Mater Res Bull* 1997;**32**:1003–8.
25. Luo J, Chiang YM, Cannon RM. Nanometer-thick surficial films in oxides as a case of prewetting. *Langmuir* 2005;**21**:7358–65.
26. Tang M, Ramos AV, Jud E, Chung SY, Gautier-Soyer M, Cannon RM, et al. Nanometer-scale wetting of the silicon surface by its equilibrium oxide. *Langmuir* 2008;**24**:1891–6.
27. Luo J, Tang M, Cannon R, Carter CW, Chiang YM. Pressure-balance and diffuse-interface models surficial amorphous films. *Mater Sci Eng A* 2006;**422**:19–28.
28. Clarke DR. On the equilibrium thickness of intergranular glass phases in ceramic materials. *J Am Ceram Soc* 1987;**70**(1):15–22.
29. Luo J. Stabilization of nanoscale quasi-liquid interfacial films in inorganic materials: a review and critical assessment. *Crit Rev Sol State Mater Sci* 2007;**32**(1):67–109.
30. Luo J, Chiang YM. Wetting and prewetting on ceramic surfaces. *Ann Rev Mater Res* 2008;**38**:227–49.
31. Luo J. Liquid-like interface complexion: from activated sintering to grain boundary diagrams. *Curr Opin Sol State Mater Sci* 2008;**12**:81–8.
32. Kofke DA, Glandt ED. Getting the most from molecular simulation. *Mol Phys* 1988;**64**:1105–31.
33. Frenkel D, Smit B. *Understanding molecular simulation: from algorithms to applications*. 2nd ed. London: Academic Press; 2002.
34. Hitchcock MR, Hall CK. Solid-liquid phase equilibrium for binary Lennard–Jones mixtures. *J Chem Phys* 1999;**110**:11433.
35. Czwartos J, Coasne B, Gubbins KE, Hung FR, Sliwinska-Bartkowiak M. Freezing and melting of azeotropic mixtures confined in nanopores: experiment and molecular simulation. *Mol Phys* 2005;**103**:3103–13.
36. Oyama T, Yoshiya M, Matsubara H, Matsunaga K. Numerical analysis of solute segregation at Σ5 (3 1 0)/0 0 1 symmetric tilt grain boundaries in Y_2O_3-doped ZrO_2. *Phys Rev B* 2005;**71**:224105.
37. Yoshiya M, Tanaka I, Adachi H. Energetical role of modeled intergranular glassy film in Si_3N_4–SiO_2 ceramics. *Acta Mater* 2000;**48**: 4641–5.
38. Toth GI, Granasy L. Phase field theory of interfaces and crystal nucleation in a eutectic system of fcc structure: II. Nucleation in the metastable liquid immiscibility region. *J Chem Phys* 2007;**127**: 044709.
39. Mellenthin J, Karma A, Plapp M. Phase-field crystal study of grain-boundary premelting. *Phys Rev B* 2008;**78**:184110.
40. Besold G, Mouritsen OG. Grain-boundary melting: a Monte Carlo study. *Phys Rev B* 1994;**50**:6573–6.
41. Hudsona TS, Nguyen-Manh D, van Duin ACT, Sutton AP. Grand canonical Monte Carlo simulations of intergranular glassy films in (-silicon nitride. *Mater Sci Eng A* 2006;**422**:123–5.
42. Swiler TP, Loehman RE. Molecular dynamics simulations of reactive wetting in metal–ceramic systems. *Acta Mater* 2000;**48**: 4419.
43. Yoshiya M, Tatsumi K, Tanaka I, Adachi H. Theoretical study on the chemistry of intergranular glassy film in Si_3N_4–SiO_2 ceramics. *J Am Ceram Soc* 2002;**85**:109–12.
44. Zykova-Timan T, Ceresoli D, Tartaglino U, Tosatti E. Physics of solid and liquid alkali halide surfaces near the melting point. *J Chem Phys* 2005;**123**:164701.
45. Zhang S, Garofalini SH. Molecular dynamics simulation of calcium diffusion in the calcium alumino-silicate intergranular films between different alumina grains. *J Am Ceram Soc* 2005;**88**:3162–9.
46. Dash JG, Fu H, Wettlaufer JS. The premelting of ice and its environmental consequences. *Rep Prog Phys* 1995;**58**:115–67.